Hand-held XRF sorting of spent refractory bricks to aid recycling

by N.P. Mabasa[1,2], N. Naudé[1], and A.M. Garbers-Craig[1]

Affiliation:
[1]Department of Materials Science and Metallurgical Engineering, University of Pretoria, Pretoria, South Africa.
[2]BEng(Metallurgy) Final Year Project Student.

Correspondence to:
A.M. Garbers-Craig

Email:
Andrie.Garbers-Craig@up.ac.za

Dates:
Received: 30 Nov. 2021
Revised: 20 Sept. 2022
Accepted: 10 Oct. 2022
Published: January 2023

How to cite:
Mabasa, N.P., Naudé, N., and Garbers-Craig, A.M. 2023 Hand-held XRF sorting of spent refractory bricks to aid recycling. Journal of the Southern African Institute of Mining and Metallurgy, vol. 123, no. 1, pp. 9–18

DOI ID:
http://dx.doi.org/10.17159/2411-9717/1928/2023

ORCID:
N. Naudé
http://orcid.org/ 0000-0002-9615-0243
A.M. Garbers -Craig
http://orcid.org/0000-0002-0298-8097

Synopsis

An improved methodology is presented for assessing the economic feasibility and effectiveness of recycling MgO-C and Al_2O_3-MgO-C refractory bricks, which are widely used in the steelmaking industry. Since approximately 28 Mt of refractory bricks are discarded each year, it is logical to recycle them. When furnaces and ladles are relined, the spent refractory bricks become mixed up, and need to be sorted before recycling. This study examined the use of a hand-held X-ray fluorescence analyser (HH-XRF) to distinguish between spent oxide-based and oxide-carbon-based refractory materials, with special emphasis on spent MgO-C (MC) and Al_2O_3-MgO-C (AMC) bricks. HH-XRF analysis was conducted on 18 oxide-carbon refractory bricks as well as on MgO-chromite and bauxite-based refractories. X-ray diffraction, reflected light optical microscopy, and scanning electron microscopy with energy dispersive spectroscopy were used to characterize the MgO-C and Al_2O_3-MgO-C bricks to confirm the accuracy of the HH-XRF analyses.

This study also underlined the importance of calibrating the HH-XRF analyser for the refractory bricks to be sorted. The HH-XRF was successful in distinguishing between the different oxide-carbon-based refractory bricks both before and after cleaning. This result is important as it proves that HH-XRF provides a method whereby spent MC and AMC bricks can be sorted quickly and reliably.

Keywords

hand-held XRF (HH-XRF), recycling, MgO-C, Al_2O_3-MgO-C, refractory bricks.

Introduction

Fang, Smith, and Peaslee (1999) define refractories as 'ceramic materials that are designed to withstand a variety of severe service conditions including high temperatures, corrosive liquids and gases, abrasion, mechanical and thermal induced stress'. According to a study conducted by Horckmans *et al.* (2019), approximately 35-40 Mt/a of refractories are produced worldwide, of which 70% goes to the iron and steel industry. It was also estimated that 28 Mt of spent refractories are generated every year. Due to factors such as increasing landfilling costs and environmental concerns (Gokce *et al.*, 2008), the need for recycling of refractory materials has increased over the years.

MgO-C (MC) bricks are of utmost importance in the steel industry where they are used in the working lining of basic oxygen furnaces, electric arc furnaces, ladle furnaces, and secondary steelmaking ladles where their high resistance to thermal spalling and corrosion is exploited (Kangal, Forssberg, and Hammergren, 2006). Al_2O_3-MgO-C (AMC) bricks, however, make up a small portion of the working lining of the electric arc furnace (EAF), where they are used in the hearth, as well as in steelmaking ladles. Since the iron and steel industry is the main consumer of refractory materials, it is understandable that this sector is the main focus of refractory recycling efforts.

Recycled MC bricks can be used as a slag conditioner, whereby the required fluxes are reduced and foaming conditions are improved, or they can be used to produce magnesia refractories (Arianpour, Kazemi, and Fard, 2009). However impurities such as slag, metal, and other foreign materials penetrate and react with the bricks during service. Spent MC bricks cannot therefore be recycled directly into fluxes or new bricks but must first be separated from other types of oxide-carbon bricks (such as AMC bricks) and cleaned (Viklund-White, Johansson, and Ponkala, 2000). Since MC and AMC bricks look similar to the naked eye, the first challenge is to separate them from each other.

For many years, manual sorting, which depends on visual identification and expertise, has been used to distinguish between refractories. There is, however, a demand for using more scientific and automated methods to improve the accuracy and speed of sorting (Horckmans *et al.*, 2019). The methods that have been investigated include a charge-coupled device (CCD) camera and laser induced breakdown spectroscopy (LIBS). This paper focuses on the use of a hand-held X-ray fluorescence analyser (HH-XRF) to distinguish between different types of oxide and oxide-carbon refractory bricks.

Background

MgO-C vs. Al_2O_3-MgO-C refractory bricks

MC bricks are unfired refractories, generally constituted from high-purity MgO aggregate (sintered or fused), graphite, a carbon binder, and powdered antioxidants such as aluminium (Al), silicon (Si), silicon carbide (SiC), boron carbide (B_4C), and Al-Si and Al-Mg alloys, which are added to protect the carbon against oxidation. Carbon is added to these bricks as a bonding phase and as graphite flakes to improve thermal shock resistance and to prevent wetting of the brick by slag, thus improving corrosion resistance.

AMC refractories are constituted from the same raw materials as the MC bricks, but also contain alumina aggregate (bauxite and corundum). They also have a continuous matrix which contains the resin binder, graphite flakes, and antioxidant additives (Munoz and Tomba Martinez, 2012). Wear is reduced due to controlled residual expansion by *in-situ* spinel ($MgAl_2O_4$) formation, which improves resistance to thermal shock and spalling (Munoz, Pena, and Tomba Martinez, 2014).

Chemical properties

The chemical composition ranges of typical synthetic resin-bonded MC and AMC bricks, without antioxidant additions, are shown in Tables I and II. The magnesia grains are of high purity (fused and/or sintered) with small amounts of impurity oxides such as alumina (Al_2O_3), haematite (Fe_2O_3), lime (CaO), and silica (SiO_2). The carbon is usually added as graphite, with carbon contents ranging from 7 to 25%. Steelmaking ladles can contain up to 12% carbon (Kujur *et al.*, 2018). AMC bricks with varying Al_2O_3: MgO ratios are produced. The impurity oxides present are governed by the amounts and types of alumina and magnesia raw materials used. Natural graphite also contributes oxide-based impurities to these bricks.

Table I

Chemical composition ranges of synthetic resin-bonded MC bricks without antioxidants, (mass%) (Routschka and Wuthnow, 2012)

MgO	Al_2O_3	C	SiO_2	Fe_2O_3	CaO
92-99	0.1-0.8	7-25	0.2-1.5	0.2-1.0	0.6-3

Table II

Chemical composition ranges of AMC bricks without antioxidants, (mass%) (Routschka and Wuthnow, 2012)

	Al_2O_3	MgO	C	SiO_2	Fe_2O_3	TiO_2
MgO <15 mass%						
Corundum	>70	<15	>2.0 – 15	<1.5	<0.3	<0.3
Bauxite	>65	<15	>2.0 – 15	<3.5	<1.0	<3.0
MgO 15 – 30 mass%						
Corundum	>55	≤30	>2.0 – 15	<1.0	<0.3	<0.3
Bauxite	>50	≤30	>2.0 – 15	<3.0	<1.0	<2.0

Effect of antioxidants on microstructure

Antioxidants protect carbon against oxidation by reacting with the carbon or the gaseous atmosphere to form carbides, oxides, and nitrides. These compounds crystallize as plates or whiskers and fill the pores or react with Al_2O_3 or MgO to form new solid phases such as spinel ($MgAl_2O_4$) or forsterite (Mg_2SiO_4), depending on the antioxidant(s) added (Munoz, Pena, and Tomba Martinez, 2014). Al and Si powders are mostly used due to their low cost and effective protection (Bag, 2011).

Zhang, Marriott, and Lee (2001) examined reactions at 1200°C for 3 hours in an MC brick in which aluminium was used as an antioxidant (Figure 1). Aluminium remained as angular, unreacted metallic particles, while it also reacted with carbon to form spheroidal Al_4C_3 and in certain areas it oxidized to form spheroidal Al_2O_3 grains. Cubic MA spinel subsequently formed through the reaction of the oxidized Al antioxidant (Al_2O_3) and MgO at approximately 1200°C. AlN formed as 10 µm diameter whiskers between graphite flakes and on the Al_4C_3 grain surfaces (Figure 1).

When Si was added as an antioxidant it also formed an oxide, a carbide, and a nitride during reaction, similar to the Al antioxidant. Forsterite was observed (Figure 2a), a SiO_2 shell surrounding the unreacted Si particle (Figure 2b), spheroidal SiC (Figure 2a-c); as well as Si_3N_4 as 10 µm black whiskers within the SiC grains (Figure 2c) (Zhang, Marriott, and Lee, 2001).

Munoz, Pena, and Tomba Martinez (2014) investigated the physical, chemical, and thermal characterization of different AMC refractories using several techniques such as XRF, XRD, reflected light optical microscopy, SEM, and gravimetry. The microstructures of the used AMC brick obtained by optical microscopy contained a large amount of alumina, with smaller proportions of antioxidant particles, and impurities such as mullite ($3Al_2O_3.2SiO_2$), tielite ($Al_2O_3.TiO_2$), and rutile (TiO_2), (Figure 3).

Market analysis

One of the most important refractory raw materials is magnesia, which accounts for 25–30% of the total refractory mineral demand. China is one of the largest suppliers of dead-burnt and fused magnesia and controls 71.3% of of the global supply of natural graphite, 65% of the synthetic graphite, and 100% of the spherical graphite (IMFORMED, 2021). Over 82.4 Mt of bauxite was exported by Guinea in 2020, making it one of the world's single largest exporters (Artacho, 2021).

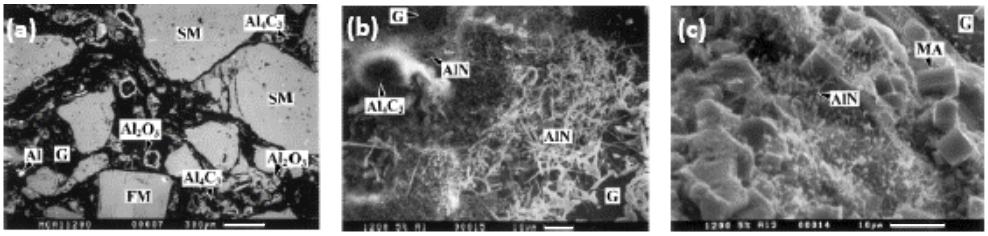

Figure 1—Microstructures of an MC brick with Al addition after 3 hours at 1200°C, (a) BEI at 300 µm; (b) and (c) secondary electron image (SEI) at 10 µm (Zhang, Marriott, and Lee, 2001) (G Graphite, FM fused magnesia, SM sintered magnesia, MA $MgAl_2O_4$)

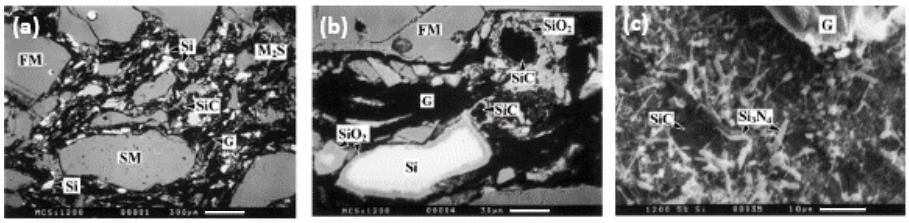

Figure 2—Microstructures of an MC brick with Si addition after 3 hours at 1200°C, (a) BEI at 100 µm; (b) BEI at 30 µm; (c) SEI at 10 µm (Zhang, Marriott, and Lee, 2001) (G Graphite, FM fused magnesia, SM sintered magnesia, M2S forsterite)

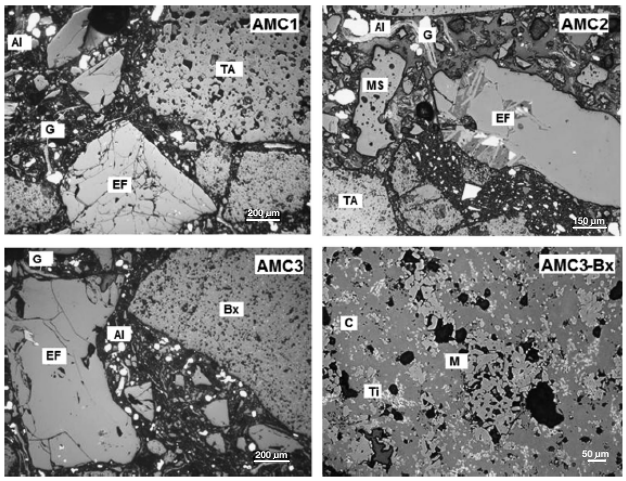

Figure 3—Reflected light microscopy images of different AMC refractories (Munoz, Pena, and Tomba Martinez, 2014) (Bx bauxite, C corundum, EF electrofused alumina, G graphite, M mullite, MS sintered magnesia, TA tabular alumina, Ti tielite)

China's exports of dead-burnt and fused magnesia were 131 kt, fused alumina 44 kt, and graphite 21 kt in February 2021 (Shaw, 2021). Graphite had the highest average economic value, followed by fused alumina (Figure 4). Magnesia had the lowest average economic value; however it is important to note that the demand for magnesia is the highest, therefore making it one of the most valuable raw materials. Recycling of MgO-containing refractories therefore has, apart from environmental benefits, great economic potential.

Experimental

Brick sampling

Oxide-carbon bricks of different colours were sampled from a heap of mixed oxide-carbon bricks at Philmar Consulting in Meyerton (Figure 5). A sample of 36 bricks was chosen at random from different positions in the heap, *i.e.*, 8 from the top, 12 from the middle, and 16 from the bottom. When sampling the bricks, it was observed that the bricks were of different sizes, shapes, and appearances (Figure 6).

Each of the bricks was numbered (including the various faces of the bricks) in order to keep track of where each individual brick (or brick face) was analysed with the HH-XRF and sampled for XRD and SEM-EDS analyses.

HH-XRF analysis of the bricks

A HH-XRF is a portable device that can be used to determine the elemental composition of materials. The HH-XRF is typically used in material science, research, and exploration geology. It can also be used in the food industry for foreign body identification and quality

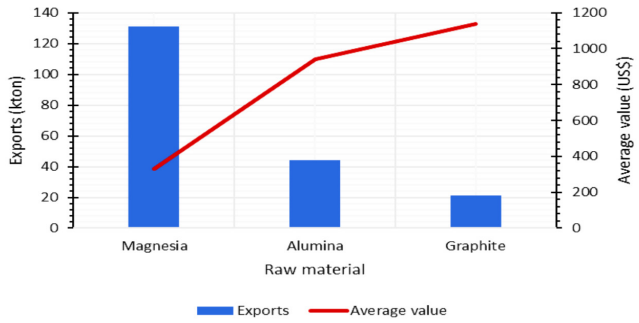

Figure 4—China's exports of magnesia, alumina, and graphite by quantity and average value, February 2021 (Shaw, 2021)

Figure 5—Heap of mixed used oxide-carbon refractory bricks

Figure 6—Used oxide-carbon bricks showing differences in size, shape, and appearance of the hot face

analysis of food, art conservation and authentication, as well as in archaeological studies for analysis of objects (Berg Engineering, 2020).

The HH-XRF is mostly used for field-testing, allowing the operator to remain mobile in the area of interest for maximum efficiency. Its features include a pistol grip and trigger-style switch, full colour displays, and it is battery operated (Drake, 2015). The main benefit of the HH-XRF is that it does not require sample preparation, and the analysis can be done rapidly (Desroches *et al.*, 2018). The size of the spot to be analysed can be varied between 1 mm and 8 mm depending on the collimators used. Additional advantages of the HH-XRF device is that it gives quick results, there are no restrictions on the number of tests that can be run, procedures can be changed without any preparation, and the device is cost-effective for most applications (Bosco, 2013).

A HH-XRF can analyse elements as light as magnesiuim and as heavy as uranium, which provides researchers with a powerful tool (Berg Engineering, 2020). It is supplied as a ready-to-use analytical instrument as it is factory-calibrated, using specific standards based on customer needs. A shortcoming of the HH-XRF is that its calibration is limited to matrices of packed powders, therefore when measuring samples that are more metallic, the increase in density results in poor calibration.

HH-XRF instruments are safe to use if used correctly. Safety precautions associated with using HH-XRF devices are mainly related to the prevention of radiation exposure (Liddle, 2012). These include holding the instrument by its handle during operation, never aiming the device at a person, never holding samples or placing samples against any body part during analysis, being aware that the primary beam can be transmitted through a work surface onto the operator's body, and ensuring that the instrument is placed against a flat surface during analysis to prevent scatter radiation from escaping.

A 4W Bruker Tracer5i HH-XRF, with a Rh anode, a SDD detector and 8mm collimator was used to analyse the bricks. The GeoMining Oxide Concentrates factory calibration was used in all cases. This factory calibration analyses for all elements between Mg and U, using three different sets of conditions to cover the entire range between Mg and U – 15 kV with no filter for the light elements, 30 kV with an AlTi filter for transition elements, and 50 kV with an AlTiCu filter for heavy elements. Carbon does not provide enough fluorescence yield to be analysed. In the oxide calibrations, no normalizations are done, so the carbon content does not affect the analyses but only causes low analytical totals. Since an initial round of analyses showed large discrepancies, the factory calibration was optimized by doing a type standardization. This was done using pressed pellets of certified refractory reference materials to compensate for the fact that the factory calibration was performed on packed powders while the analyses were directly on bricks with very different densities. The HH-XRF analyses were repeated three times on two faces that were identified as either the hot face or the cold face of the brick. The analyses were conducted on the spots and faces shown in Figure 7. The as-received bricks were analysed and after observing the effect that dust had on brick 9 (especially as regards to the light elements), the bricks were cleaned by dusting with a brush on each of the faces (hot face and cold face) prior to analysis. Each spot was analysed once.

Sample preparation for XRD and SEM-EDS analyses

A characterization study was conducted to determine the validity of the HH-XRF results, *i.e.*, if the HH-XRF can undeniably distinguish between MC and AMC bricks. The purpose of the XRD and SEM/EDS analyses was to obtain a basic understanding of the phases present in the bricks, as this information is important when interpreting the HH-XRF data. For example, when a discard MC brick, which contained aluminium as anti-oxidant, is analysed with XRF, the reported aluminium concentration will be low (< 5 mass%), while the aluminium concentration of a discard AMC brick (with aluminium anti-oxidant) will be high (> 50 mass%). XRD and SEM/EDS analyses give supplementary information on whether the reported aluminium is present in metallic, carbide, or oxide forms, or in combinations thereof.

The bricks were cut using a diamond blade circular saw close to one of the spots that were analysed by the HH-XRF. The sectioned part was cut into two, one half was prepared for XRD and the other was prepared for SEM/EDS analysis (Figure 8). Each brick sample cut for XRD analysis was hammered and then pulverized to –75 µm (Figure 9). XRD analysis was performed using a PANalytical X'Pert Pro powder diffractometer.

To prepare the brick samples for SEM/EDS and light optical microscopy, 10 parts of epoxy resin to 6 parts hardener were mixed and poured into a mould containing the brick samples. The mounted samples were then put under vacuum for 10 minutes to eliminate trapped air in the mixture and left to dry overnight in an oven at 40°C. The samples were polished and then gold coated before SEM/EDS analysis using a Jeol JSM–IT300LV scanning electron microscope coupled with an Oxford X–Max 50 energy–dispersive X–ray spectrometer.

Results and discussion

Characterization using XRD analysis

The relative phase amounts (weight%) of the crystalline portions of bricks 14, 26, and 29 were estimated from the hot and cold faces of each of the bricks using the Rietveld method (X'Pert Highscore Plus software) (Table III). The major crystalline phase in brick 14 was periclase (MgO), while forsterite (Mg_2SiO_4) and monticellite ($CaMgSiO_4$) were identified as minor phases. Monticellite is an impurity phase associated with MgO aggregate originating from magnesite ($MgCO_3$). In brick 29, periclase was also identified as a major phase. The minor phases were monticellite, magnetite (Fe_3O_4), and forsterite. Graphite was absent in both bricks 14 and 29. This was confirmed by the light brown colour of the pulverized samples, which indicated that these were magnesia bricks that ended up on the oxide-carbon brick dump. Two major phases were identified in brick 26 – periclase and graphite.

SEM/EDS

Typical microstructures of the MC and AMC bricks are shown in Figure 10. MgO aggregates were identified in the MC bricks whereas alumina and MgO aggregates were identified in AMC bricks, as expected. Monticellite, merwinite, and forsterite were observed in the MC brick, while phases such as tielite and alumina-silicates were observed in the AMC brick. Forsterite presumably formed after the Si antioxidant and / or formed SiC oxidized to silica (SiO_2) and reacted with MgO according to Equations [1]-[4]:

$$Si_{(s)} + 2CO_{(g)} \rightarrow SiO_{2(s)} + 2C(s) \quad [1]$$

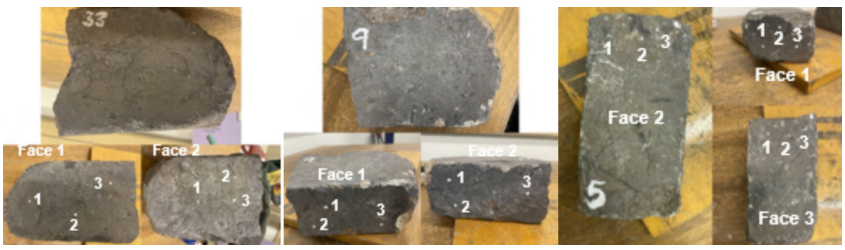

Figure 7—Brick samples showing the faces and spots that were analysed using the HH-XRF

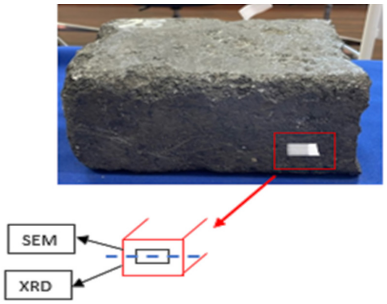

Figure 8—Illustration of how each brick was cut and sampled for XRD and SEM/EDS analyses

Figure 9—Pulverized brick samples for XRD analysis

$$Si_{(s)} + C_{(s)} \rightarrow SiC_{(s)} \quad [2]$$

$$SiC_{(s)} + 2CO_{(g)} \rightarrow SiO_{2(s)} + 3C_{(s)} \quad [3]$$

$$SiO_{2(s)} + 2MgO_{(s)} \rightarrow Mg_2SiO_{4(s)} \quad [4]$$

XRD and SEM-EDS analyses confirmed that the majority of elements detected in the bricks were present as oxides. The HH-XRF data was therefore expressed as oxides, *i.e.* MgO, Al_2O_3, SiO_2, CaO, Fe_2O_3 / Fe_3O_4, Cr_2O_3, and TiO_2.

Sorting

Effect of dusting of the bricks before HH-XRF analysis

Brick 9 was used to investigate the effect of dusting of the bricks on the HH-XRF results (Figure 11, Table IV). The SiO_2 content (probably originating from dust) decreased, whereas the MgO content and total chemical composition increased after the brick was cleaned with a brush. This was an indication that the amount of dust on the brick adversely affects the accuracy of the MgO analysis (an element with a low atomic mass).

Repeatability of the HH-XRF results

The repeatability of the HH-XRF analyses was determined by analysing a single spot (spot 1) ten times and the reproducibility of analysis *i.e.* homogeneity of the brick was evaluated by analysing 10 different spots on brick 6 (Figure 12). Figure 13 shows the results. The chemical composition of the brick seemed homogeneous with the naked eye (Figure 14), but the HH-XRF results showed a significant variation in MgO content (standard deviation of 6% when 10 different spots were analysed). This presumably is due to a large MgO aggregate grain (3 mm in diameter) sometimes

Table III

Mass percentage of crystalline phases estimated using the Rietveld method

		Periclase	Monticellite	Magnetite	Forsterite	Graphite
Brick 14	Cold face	96.50	-	1.17	2.33	-
	Hot face	95.2	2.4	1.17	2.4	0
Brick 26	Cold face	94.00	-	-	-	6.00
	Hot face	91.3	-	-	-	8.7
Brick 29	Cold face	96.45	1.79	0.16	1.61	-
	Hot face	96.1	1.4	0.16	2.5	0.0

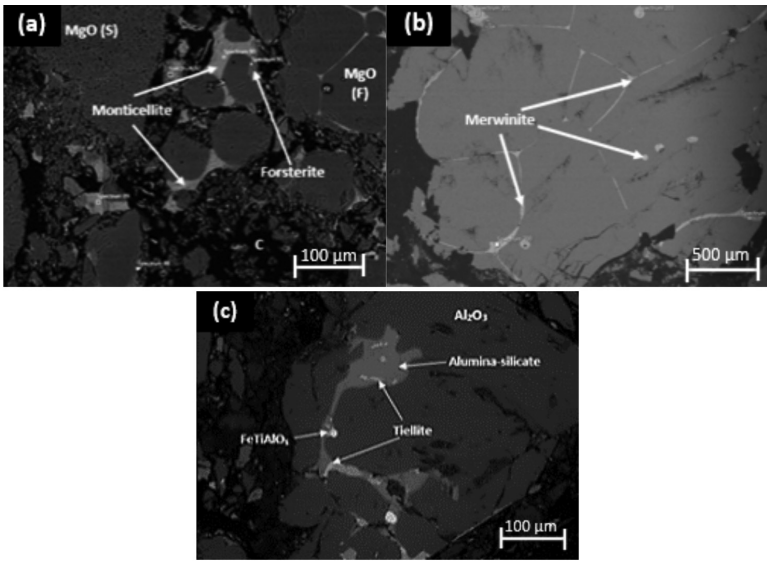

Figure 10—Backscattered electron images of MC refractory bricks (a) and (b) and AMC refractory brick (c). Periclase: MgO; monticellite: $CaMgSiO_4$; forsterite: Mg_2SiO_4; graphite: C; merwinite ($Ca_3MgSi_2O_8$); tielite (Al_2TiO_5)

falling within (or partially within) the collimated spot analysed. In contrast, when the same spot was analysed 10 times the compositional variation was insignificant. For this scenario, the MgO content had the highest variation of all the oxides, but with a standard deviation of only 1%, which is well within the analytical uncertainty associated with Mg analyses by HH-XRF.

HH-XRF analysis of 15 oxide-carbon bricks

The factory-calibrated HH-XRF was used to analyse 15 clean oxide-carbon bricks (Figure 15). High percentages of MgO were recorded, as expected from an MC brick. Although significant variations were observed, as indicated by the error bars, the HH-XRF was able to identify MC bricks.

The oxide composition of brick 14 was estimated through a mass balance calculation of the crystalline phases identified using quantitative XRD and compared with the HH-XRF results (Table V). A significant difference was observed in the MgO, SiO_2, and CaO contents determined by the two methods.

It is assumed that the accuracy of the HH-XRF data could have been affected by sample preparation (samples were analysed as received and not pulverized), the fact that characteristic X-ray photons are emitted from only the top few micrometres of the sample, especially in the case of light elements, the fact that the HH-XRF cannot analyse for carbon, and that the HH-XRF was not calibrated for the types of refractory bricks used in this study.

HH-XRF analysis of oxide-based refractory bricks

After it was realized that all the oxide-carbon brick samples from the stockpile were MC bricks, which again highlights the difficulty of distinguishing between the MC and AMC bricks, a test was conducted on previously characterized virgin refractory bricks (magnesia-chromite, bauxite-based bricks). These tests were aimed at determining if the HH-XRF was able to distinguish between different oxide-based refractory bricks, *i.e.* bricks that do not contain any carbon. The macrostructures of these bricks, as can be seen with the naked eye, are shown in Figure 16.

Magnesia-chromite brick compositions reported by the HH-XRF were similar to the expected MgO and Cr_2O_3 compositions of 52% and 26% respectively. The alumina content of the bauxite brick was close to the expected 83%; however, the SiO_2 content was too high (Table VI).

HH-XRF analysis of the MC and AMC refractory bricks

The MC and AMC refractory bricks that were characterized using XRD and SEM-EDS were also analysed with the HH-XRF. The HH-XRF reported 100% alumina (Table VII), which was much higher than the expected 67% (Table VIII) and completely unrealistic.

Figure 11—Dusting of bricks

Figure 12—Brick 6 face1 used to test for repeatability of the HH-XRF results

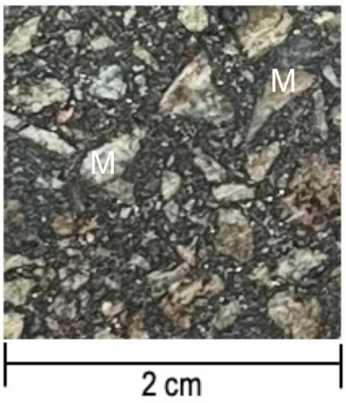

Figure 14—Macrostructure of the virgin MC refractory brick: MgO grains embedded in a carbon-bonded matrix which contains MgO fines, graphite flakes, and Al antioxidant particles (M = MgO grains)

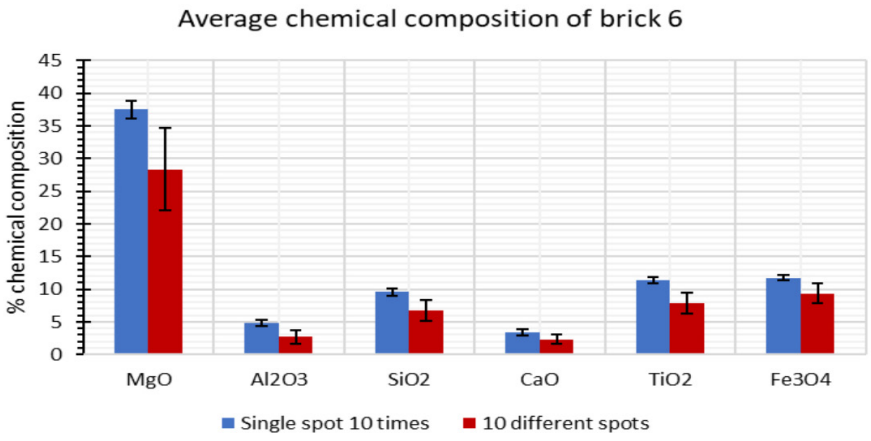

Figure 13—Average chemical composition with standard deviations of brick 6

Table IV

HH-XRF results obtained for brick 9 before and after cleaning

	Chemical composition (mass%)								
Brick 9 Spot1	**MgO**	**Al_2O_3**	**SiO_2**	**CaO**	**TiO_2**	**Cr_2O_3**	**MnO**	**Fe_3O_4**	**Total**
Dusty	20.69	3.04	9.96	6.81	16.97	0.14	0.75	17.32	75.68
Clean	32.07	3.98	6.93	6.46	17.66	0.14	0.48	11.57	79.29

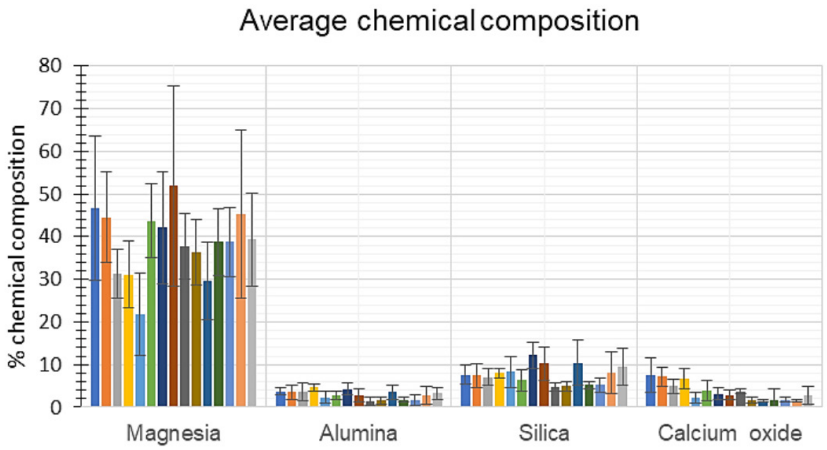

Figure 15 —HH-XRF average chemical composition of 15 clean oxide-carbon bricks

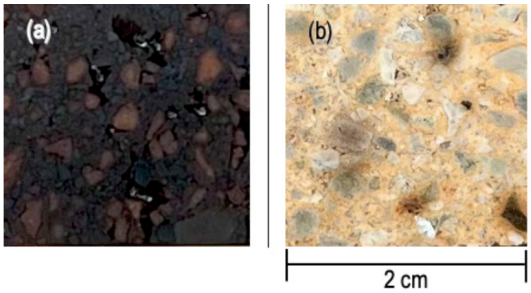

Figure 16—Macrostructures of the virgin oxide refractory bricks: (a) magnesia-chromite brick, (b) bauxite-based brick

Table V

HH-XRF analyses *vs.* calculated chemical compositions of bricks 14, 26 and 29 (mass%)

	MgO	SiO_2	CaO	Graphite
Brick 14				
HH-XRF	21.87	8.31	2.36	-
XRD: Cold face	97.64	1.37	0.42	-
XRD: Hot face	96.71	1.90	0.91	-
Brick 26				
HH-XRF	36.39	4.92	1.8	-
XRD: Cold face	94.00	-	-	6
XRD: Hot face	91.30	-	-	8.7
Brick 29				
HH-XRF	29.67	10.40	1.50	-
XRD: Cold face	97.54	1.34	0.64	-
XRD: Hot face	97.40	1.54	0.50	-

The MgO concentration reported by the HH-XRF in the MC brick (Table VII) was higher than the expected 88% (Table IX).

HH-XRF analysis of an AMC refractory brick before and after calibration

Due to the high alumina reported in the previous tests, it was clear that the factory-calibrated HH-XRF was not suitable for analysis of the refractory bricks, as it was calibrated for a maximum of 69% Al_2O_3. Pressed powders of refractory brick reference materials were therefore prepared (Figure 17) and analysed in order to carry out a 'type standardization' (an empirical correction method used to optimize HH-XRF equipment for specific matrices) to improve accuracy. The AMC brick was analysed again, and values close to the data sheet values in Table VIII were obtained (Table X), indicating that a type standardization can be used to improve quantitative HH-XRF results.

Effect of reducing HH-XRF analysis time

Apart from accuracy, the speed of sorting through the spent refractories is important, hence the effect of reducing the analysis time on a single brick was investigated (Table XI). The measurement time was reduced from 90 seconds to 50 seconds. Although the measured magnesia content decreased, the type of brick could still be identified. Therefore, a HH-XRF can also be used at measurement times of 50 seconds, thus permitting the sorting of refractory bricks at a faster pace.

Conclusions

- HH-XRF technology can successfully distinguish between different types of oxide-based and oxide-carbon-based refractory bricks.
- It is important to calibrate the HH-XRF using refractory brick reference materials before analysis (sorting) is started, as the factory calibration is not sufficient.

Table VI

HH-XRF test results for oxide-based refractories

Test brick	Chemical composition (mass%)							
	MgO	Al_2O_3	SiO_2	CaO	TiO_2	Cr_2O_3	Fe_2O_3	Total
HH-XRF analysis of MgO-chromite brick	54.67	6.12	2.91	0.00	0.10	19.25	7.75	92.04
Expected concentrations from the data sheet	52.00	10.00	0.80	0.80	-	26.00	11.00	100.60
HH-XRF analysis of bauxite brick	0.73	88.00	22.55	0.62	3.02	0.08	0.95	117.62
Expected concentrations from the data sheet	-	83.00	-	-	2.80	-	1.40	

Table VII

HH-XRF test results for the virgin MC and AMC bricks

Test brick	Chemical composition (mass%)							
	MgO	Al_2O_3	SiO_2	CaO	TiO_2	Cr_2O_3	Fe_2O_3	Total
AMC	45.04	100.00	11.75	0.63	1.67	0.03	0.00	159.12
MC	91.09	11.75	6.82	0.92	0.01	0.03	0.60	111.22

Table VIII

Composition of the AMC brick, as reported in the data sheet

	Chemical composition (mass%)					
Brick	MgO + CaO	Al_2O_3	SiO_2	$K_2O + Na_2O$	TiO_2	Fixed carbon
AMC	13.56	67.00	8.97	0.10	2.53	6.88

Table IX

Composition of the MC brick, as reported in the data sheet

	Chemical composition (mass%)					
Brick	MgO	Al_2O_3	SiO_2	CaO	Fe_2O_3	Fixed carbon
MC	88.00	9.00	3.00	0.92	0.25	14.00

Table X

HH-XRF analysis of an AMC refractory brick before and after type standard calibration

	Chemical composition (mass%)							
AMC test brick	MgO	Al_2O_3	SiO_2	CaO	TiO_2	Cr_2O_3	Fe_2O_3	Total
Before calibration	45.04	100.00	11.75	0.63	1.67	0.03	0.00	159.12
After calibration	33.04	53.28	11.54	1.30	1.15	0.02	0.00	100.33

Table XI

HH-XRF results for an MC brick analysed for 90 seconds and 50 seconds

Analysis time	Chemical composition (mass%)							
	MgO	Al_2O_3	SiO_2	CaO	TiO_2	Cr_2O_3	Fe_3O_4	Total
90 seconds	58.19	2.69	7.74	3.10	2.73	0.13	2.40	76.98
50 seconds	36.65	2.76	7.93	4.62	2.12	0.13	2.43	56.64

Figure 17—Pressed powders of refractory brick reference materials

- The spot size analysed with the HH-XRF should be as large as possible relative to the largest size fraction of aggregate material used in the brick formulation.
- Although dusting of the bricks increases quantitative accuracy, it was shown that even without cleaning one can still distinguish between different types of oxide-carbon refractories.
- HH-XRF is a reliable and quick technique by which MC and AMC bricks can be sorted before their different raw materials are recovered and recycled.

Acknowledgements

The authors gratefully acknowledge Vesuvius South Africa and Philmar Consulting for providing the oxide-carbon refractory bricks. Special thanks are also due to Maggi Loubser from the School of Arts at the University of Pretoria for the use of the Bruker Tracer5i HH-XRF analyser as well as for technical support.

References

Arianpour, F., Kazemi, F., and Fard, F.G. 2009. An outlook of refractory recycling experience in Iran. *Proceedings of the 11th Unified International Technical Conference UNITECR 2009*, Salvador, Brazil. https://www.researchgate.net/profile/Faramarz-Kazemi/publication/324860711_AN_OUTLOOK_OF_REFRACTORY_RECYCLING_EXPERIENCE_IN_IRAN/links/5ae7f2be0f7e9b837d393c25/AN-OUTLOOK-OF-REFRACTORY-RECYCLING-EXPERIENCE-IN-IRAN.pdf

Artacho, M. 2021. Guinea-Bissau plays a crucial role in global bauxite supply chain. *Africa News*. https://www.topafricanews.com/2021/09/08/guinea-bissau-plays-a-crucial-role-in-global-bauxite-supply-chain-by-miguel-artacho/ [accessed 26 September 2021].

Bag, M. 2011. Development of environmental friendly new generation MgO-C brick using nano carbon. MTech thesis, Rourkela National Institute of Technology, India.

Berg Engineering. 2020. Bruker TRACER 5i handheld XRF analyzer (TRACER5I). https://www.bergeng.com/product/TRACER5I.html [accessed 26 September 2021]

Desroches, D., Bedard, L.P., Lemieux, S., and Esbensen, K.H. 2018. Suitability of using handheld XRF for quality control of quartz in an industrial setting. *Minerals Engineering*, vol. 126. pp. 36–43. https://doi.org/10.1016/j.mineng.2018.06.016

Drake, L. 2015. User guide: Tracer series. https://www.xrf.guru/WorkshopVI/TracerDocumentation/Manuals/files/Tracer%20User%20Guide.pdf [accessed 26 September 2021]

Fang, H., Smith, J.D., and Peaslee, K.D. 1999. Study of spent refractory waste recycling from metal manufacturers in Missouri. *Resources, Conservation and Recycling*, vol. 25. pp. 111–124.

Gokce, A.S., Gurcan, C., Ozgen, S., and Aydin, S. 2008. The effect of antioxidants on the oxidation behaviour of magnesia-carbon refractory bricks. *Ceramics International*, vol. 34. pp. 323–330. https://doi.org/10.1016/j.ceramint.2006.10.004

Horckmans, L., Nielsen, P., Dierckx, P., and Ducastel, A. 2019. Recycling of refractory bricks used in basic steelmaking: A review. *Resources, Conservation and Recycling*, vol. 140. pp. 297–304. https://doi.org/10.1016/j.resconrec.2018.09.025

IMFORMED. 2021. Refractory minerals market: facing up to the future. http://imformed.com/refractory-minerals-market-facing-up-to-the-future/ [accessed 20 September 2021]

Kangal, O., Forssberg, E., and Hammergren, P. 2006. Evaluation of MgO-C bricks for recovering graphite and magnesite. *Proceedings of the XXIII International Mineral Processing Congress*, Istanbul, Turkey. Önal, G. (ed.). International Minerals Processing Council. pp. 2236–2244.

Kujur, M.K., Roy, I., Kumar, K., Chintaiah, P., Ghosh, S., and Ghosh, N.K. 2018. Raw materials for manufacturing of superior quality MgO-C bricks. Materials Today: Proceedings, vol. 5. pp. 2359–2366. https://doi.org/10.1016/j.matpr.2017.09.242

Liddle, S.A. 2012. Guidance on the safe use of handheld XRF analysers. Society for Radiological Protection. https://www.rp-alba.com/resources/Guidance_on_the_safe_use_of_Handheld_XRF.pdf

Muñoz, V., Galliano, P.G., Brandaleze, E., and Tomba Martinez, A.G. 2015. Chemical wear of Al_2O_3-MgO-C bricks by air and basic slag. *Journal of the European Ceramic Society*, vol. 35. pp. 1621–1635. https://doi.org/10.1016/j.jeurceramsoc.2014.11.024

Munoz, V., Pena, P., and Tomba Martinez, A.G. 2014. Physical, chemical an thermal characterization of alumina-magnesia-carbon refractories. *Ceramics International*, vol. 40, no. 7A. pp. 9133–9149. https://doi.org/10.1016/j.ceramint.2014.01.128

Routschka, G. and Wuthnow, H. 2012. Handbook of Refractory Materials - Design - Properties - Testing. 4th edn. Vulkan Verlag GmbH, Esseh, Germany.

Shaw, S. 2021. Refractories: Chinese trade data for Jan/Feb highlight raw material disruption. https://roskill.com/news/refractories-chinese-trade-data-for-jan-feb-highlight-raw-material-disruption/ [accessed 28 June 2021]

Viklund-White, C., Johansson, H., and Ponkala, R. 2000. Utilization of spent refractories as slag formers in steelmaking. *Proceedings of the 6th International Conference on Molten Slags, Fluxes and Salts*, Stockholm, Sweden and Helsinki, Finland. https://www.pyrometallurgy.co.za/MoltenSlags2000/pdfs/212.pdf

Zhang, S., Marriott, N.J., and Lee, W.E. 2001. Thermochemistry and microstructures of MgO-C refractories containing various antioxidants. *Journal of the European Ceramic Society*, vol. 21, no. 8. pp. 1037–1047. https://doi.org/10.1016/S0955-2219(00)00308-3 ◆